Internal Crack Detection in Concrete Pavement using Discrete Strain Sensors

Mohanad Alshandah [1], Ying Huang [1]*, Zhili Gao[2], and Pan Lu[3]
[1] Dept. of Civil and Environmental Engineering, North Dakota State University, Fargo, United States, 58108-6050, U.S.A
[2] Dept. of Construction Engineering and Management, North Dakota State University, Fargo, United States, 58108-6050, U.S.A
[3] Dept. of Transportation Logistics, Logistics, and Finance, North Dakota State University, Fargo, United States, 58108-6050, U.S.A

Abstract Cracking in concrete pavements is a major concern for their performance, especially the existence of the internal bottom-up cracks. These cracks may induce water penetration in pavement structure and foundation, resulting in pavement degradation. Early detection of the hidden cracks in concrete pavements can expedite timely maintenance, which improves the safety of the infrastructure. This paper develops a detection system for internal crack location and propagation using discrete strain sensors at the bottom of the concrete pavements. In this study, based on linear elastic fracture mechanics, a theoretical approach derived from locating the bottom-up crack and tracking the crack propagation using a minimum of two discrete in-pavement strain sensors. Experimental results showed that the proposed crack detection approach with two discrete strain sensors could detect bottom-up cracks with an average measurement accuracy of 82.4% for three specimens tested in the laboratory. This study may provide an alternative technique to detect hidden bottom-up cracks in concrete pavements.

Keywords Concrete pavement, bottom-up crack, crack detection, discrete strain sensor, stress intensity.

1 Introduction

Concrete pavements represent one of the most important components for transportation infrastructure, which directly affects the quality of transportation. With the growth of the population, road infrastructure continues to expand to accommodate the increasing growth. Besides the expanding of road networks in every decade, these systems require ongoing maintenance and repairs [1]. However, the agencies should consider components of user costs are the delayed time cost such as loss of work time, the operation cost such as cost of gas, the crash cost of vehicles, and driver tension. Traffic congestion results in and consequently contributes to increasing rates of emissions in the environment. [2]. Concrete pavement deformation by excess loads or environmental effect leads to cracking, which in turn induces significant pavement damages in addition to increased risk in road accidents and damages to the automobile. Therefore, a crack detection system to diagnose early cracking in pavements would save agencies cost and labor for maintenance [3].

Several techniques have been investigated by researchers to detect internal cracks in pavements such as; Ground Penetrating Radar (GPR) [4-9], ultrasonic technology [10-15], and in-pavement sensors [16-21]. GPR emits and measures high-frequency electromagnetic pulse waves to the measured object through the transmitting antenna. This is utilized by using the difference in the electromagnetic properties of the underground medium, reflections, and transmissions of electromagnetic waves generated at the interfaces of different electrical interfaces [4, 5]. For instance, the dielectric constants of the air and pavement are different, and the receiving antenna receives the reflected echo and records reflection time, which can use to map the cracks in a highway [6] or airport pavements and subgrades [7, 8]. The GPR can scan the pavement in three dimensions within a limited depth. Previously, GPR has been used to detect pavement distresses such as cracks, water-damage pits, and uneven settlements with 85.17% precision and 2.15 mm location errors in real-world conditions [9]. However, due to the transmission limitation of the electromagnetic waves, GPR is difficult to get an accurate estimation of cracks when the pavement is very thick, or when moistures present, or when the detection is on other interfere [4, 5].

In addition, ultrasonic technology was investigated to detect cracks and longitudinal joints in asphalt concrete pavements [10-15], through the utilization of ultrasonic reflections. In an ultrasonic system, one transducer sent out a stress-wave pulse and the second transducer received the reflected pulse, the time from the start of the pulse to the arrival of the echo was measured to estimate the crack locations [10]. With multiple arrays of probes, the ultrasonic

sensors are able to detect pavement distresses such as delamination at the mid-depth of concrete pavement slabs, spalling, and map cracking in concrete pavement slabs, and mud balls in a concrete runway [11, 12]. In addition, the recurrence plot quantification analysis (RQA) method can improve the sensitivity to damage in spoiled series, improving the reliability of damage detection with ultrasonics in non-homogeneous materials [13]. However, due to a low transmission capacity of ultrasonic waves in concrete, the detection limit of this technique is constrained by several conditions such as environment and weather change, different properties of materials could be available during the test.

In-pavement sensors can also be used to measure internal cracks in concrete pavements. One of the most popular in-pavement sensors used is the electrical resistance based strain gauge [14]. When a strain gauge is tightly bonded to a measuring object, the mechanical elongation or contraction of the bonded structure will change the electric resistance of the metal sensing element of the strain gauge, which can be measured. Strain gauges installed in asphalt pavement in airport runways successfully detected strain changes with airplane take-off and landing and potential damages over time, especially in the gauges nearest to the taxiway [14]. In addition to electrical resistance-based strain gauges, optic fiber strain gauges were also utilized to investigate crack detections such as fiber Bragg grating sensors [15] and distributed fiber optic sensors [16-18]. These fiber optic strain gauges can detect strain changes in pavements, which can be related to crack initiation in pavements. By using two fiber optic sensor nodes, information of bridge performance had been collected [19]. Also, Fiber Bragg grating (FBG) sensors can be used to monitor pavement performances in a harsh environment [20]. However, most in-pavement sensors employed to detect pavement cracks are installed near the pavement surface, preventing them from detecting cracking from bottom to up with different weather conditions, traffic, and the environmental effect.

A comparison of the currently available sensing technologies for pavement crack detection is summarized in Table 1. As can be seen from the table, the in-pavement sensors that are installed beneath the pavement surface, have a low reaction to weather conditions, relatively low cost, and no need to close traffic during measurements. Thus, if installed at the bottom of the pavements, in-pavement sensors have the most potential to detect pavement hidden cracks. For these sensors, although distributed fiber optic sensors are available [16-18], due to their high cost, their practical applications are still limited, and discrete point sensors are still dominating.

Table 1 Comparison of pavement crack detection sensing technologies

	GPR	**Ultrasonic**	**In-pavement sensors**
Application locations	Running on pavement surface	Installed on pavement surface	Can be installed on or beneath pavement surface
Durability	High impact by weather conditions	High impact by weather conditions	Low impact from weather conditions
Cost	Relatively high	Relatively high	Relatively low
Accuracy	Between 20 to 50 mm	More than 50 mm	Between 10 to 50 mm
Traffic Impact	Traffic closure required	Traffic closure required	No traffic closure needed

When applying discrete point in-pavement sensors to detect the internal cracks in concrete pavements, due to cost restrictions, only limited numbers of sensors can be deployed, and the crack may occur at a different location than that where the discrete sensor was located. Thus, using discrete sensors to detect hidden cracks in concrete is still very challenging. To meet the above mentioned challenge, this paper develops an innovative approach to localize and monitor the internal crack initialization and propagation in concrete pavement using minimum numbers of in-pavement discrete strain sensors. The developed approach is based on linear elastic fracture mechanics and was verified by laboratory experiments. Upon further field validation, the developed crack detection approach may provide an alternative method to estimate bottom-up cracks in the concrete pavement to better evaluate concrete pavements for timely maintenance. The detected bottom-up crack layout can assist an appropriate future pavement repair. In addition, these crack layout can help determine the reduced long-term durability performance and properties for concrete such as modulus of elasticity (E) and poisons ratio (υ), which can be used to improve the future pavement design procedures with consideration on pavement damages. More importantly, the developed technique can also be extended to apply in civil infrastructure with areas having limited accessibly, such as bridges,

nuclear reactors, buildings, tunnels, powerplants, and dams. The capability of detecting hidden cracks in these concrete structures with low cost is also with high demand and significance.

2 Theoretical Analysis

When placed inside the concrete pavements, discrete sensors would monitor the changes of the strain field inside the pavements. When a crack initialized, the strain distributions inside the concrete pavement will be changed and can be detected by the nearby in-pavement discrete strain sensors. To derive the theoretical transfer function between the discrete embedded strain sensors and the strain changes induced by crack initialization inside concrete pavements, it is required to analyze the stress/displacement field around cracks based on linear elastic fracture mechanics. Since concrete is a brittle material, the crack in concrete behaves elastically [21]. While in many cases the material may be ductile, the size of the plastic zone is very small, and the plastic zone can be ignored in these cases. In linear elastic fracture mechanics, the stress intensity factor (K) is used to predict the stress state, also known as "stress intensity," near the tip of a crack caused by a remote load or residual stresses. The stress intensity determines the stress and displacement fields in cracked solids near the crack tip [22, 23]. The magnitude of stress intensity factor depends on the geometry, size, and location of the crack, and the magnitude and the modal distribution of loads on the material, which can describe as:

$$K = \alpha \sigma_a \sqrt{\pi} a \tag{1}$$

where σ_a is applied stress derived from applied loads, a is the depth of the crack, and α is a parameter dependent on the size of the specimen and crack geometry [24].

Generally, there are three modes of cracks, including Mode I opening a crack, Mode II in-plane shear, and Mode III out-of-plane shear. Most internal cracks, such as bottom-up crack inside pavements, belong to Mode I opening cracks [25]. For Mode I cracks, linear elastic theory predicts that if the stress intensity factor K is known, in the condition when the loading applied on the top of the concrete pavement, the stress distribution (σ) in x directions at a random location near the crack tip, σ_x, can be estimated as [26]:

$$\sigma_x = \frac{K}{\sqrt{2\pi r}} \cos\frac{\theta}{2}\left[1 + sin\frac{\theta}{2} sin\frac{3\theta}{2}\right] \tag{2}$$

where, r and θ are the radius distance and angle between the crack tip and the random location, respectively. If the elastic modulus (E) of concrete materials is known and the concrete is assumed to be elastic, the strains in the x-direction at a random location can then estimated as:

$$\varepsilon_x = \frac{K}{E\sqrt{2\pi r}} \cos\frac{\theta}{2}\left[1 + sin\frac{\theta}{2} sin\frac{3\theta}{2}\right] \tag{3}$$

Thus, substituting Equation (1) into Equation (3), we have:

$$\varepsilon_x = \frac{\alpha \sigma_a}{E\sqrt{2r}} a \cos\frac{\theta}{2}\left[1 + sin\frac{\theta}{2} sin\frac{3\theta}{2}\right] \tag{4}$$

To measure bottom-up cracks, discrete strain sensors are recommended to be installed at the bottom of the pavements. Assuming that one crack is initialized in the perpendicular direction of the pavement bottom surface if two discrete sensors (Sensor 1 and Sensor 2) are installed and the crack is located in between the two sensors as shown in Figure 1, the distance, L, between the two sensors, when installed, is known, and equals to $L_1 + L_2$, with L_1 the distance between Sensor 1 and the crack and L_2 the distance between Sensor 2. Thus, the radius distance and angle between the crack tip and Sensor 1 is r_1, θ_1 and that between the crack tip and Sensor 2 is r_2, θ_2 as also shown in Fig. 1.

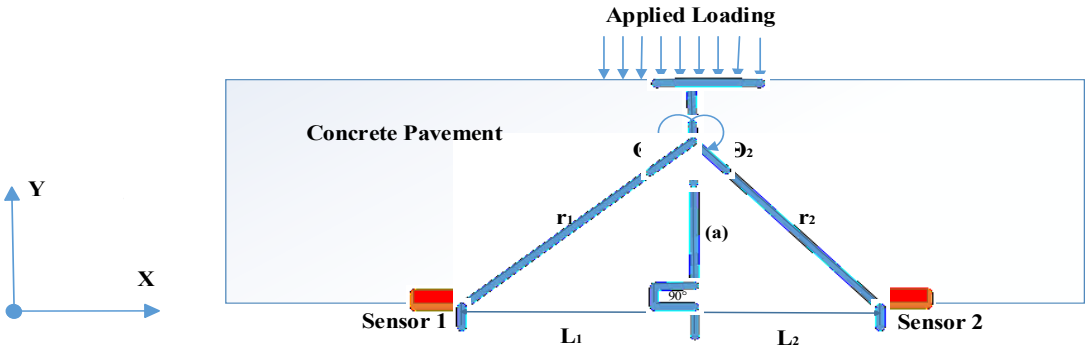

Fig. 1 Sensor locations vs. perpendicular crack

Based on the assumption that the crack is perpendicular to the bottom of the pavement, then, the geometrical relation between the crack depth (a), the radius distance (r_1), the crack radius angle (θ_1), and the distance between the Sensor 1 and the crack (L_1), can be determined as:

$$\tan(\theta_1 - 90^o) = a/L_1 \tag{5}$$

$$\cos(\theta_1 - 90^o) = L_1/r_1 \tag{6}$$

Thus, the radius distance (r_1) and the crack radius angle (θ_1) can be replaced by the crack depth (a) and the distance between the Sensor 1 and the crack (L_1) as:

$$\theta_1 = \tan^{-1}(a/L_1) + 90^o \tag{7}$$

$$r_1 = \frac{L_1}{\cos(\theta 1 - 90^o)} \tag{8}$$

Putting Equations (7, 8) into Equation (4), the measured strain at Sensor 1 location, ε_1, can be estimated as:

$$\varepsilon_1 = \frac{\sigma\sqrt{a}}{1.4142 * E * \sqrt{\frac{L_1}{\cos[\tan^{-1}\left(\frac{a}{L_1}\right)]}}} \cos\frac{\tan^{-1}[\left(\frac{a}{L_1}\right)+90^\circ]}{2}\left[1 - \sin\frac{\tan^{-1}[\left(\frac{a}{L_1}\right)+90^\circ]}{2}\sin\frac{3\tan^{-1}[\left(\frac{a}{L_1}\right)+90^\circ]}{2}\right] \tag{9}$$

Following the same procedure as for ε_1, the measured strain at Sensor 2 location can be estimated based on the crack depth (a) and the distance between the Sensor 2 and the crack (L_2) as below:

$$\varepsilon_2 = \frac{\sigma\sqrt{a}}{1.4142 * E * \sqrt{\frac{L_2}{\cos[\tan^{-1}\left(\frac{a}{L_2}\right)]}}} \cos\frac{\tan^{-1}[\left(\frac{a}{L_2}\right)+90^\circ]}{2}\left[1 - \sin\frac{\tan^{-1}[\left(\frac{a}{L_2}\right)+90^\circ]}{2}\sin\frac{3\tan^{-1}[\left(\frac{a}{L_2}\right)+90^\circ]}{2}\right] \tag{10}$$

Considering that the distance, L, between the two sensors, equals to $L_1 + L_2$, Equation (10) can be rewritten as:

$$\varepsilon_2 = \frac{\sigma\sqrt{a}}{1.4142 * E * \sqrt{\frac{L-L_1}{\cos[\tan^{-1}\left(\frac{a}{L-L_1}\right)]}}} \cos\frac{\tan^{-1}[\left(\frac{a}{L-L_1}\right)+90^\circ]}{2}\left[1 - \sin\frac{\tan^{-1}[\left(\frac{a}{L-L_1}\right)+90^\circ]}{2}\sin\frac{3\tan^{-1}[\left(\frac{a}{L-L_1}\right)+90^\circ]}{2}\right] \tag{11}$$

Thus, if the strains at Sensor locations 1 and 2 are measured, based on Equations (9, 11), the crack location, L_1, and the crack depth, a, can be estimated considering the semi-inverse method developed by Westergaard [27].

As illustrated above, Equations (9, 11) were derived based on the assumption that the crack is perpendicular to the bottom surface of the pavement. When the crack is initializing, the assumption of the perpendicular crack is reasonable. Thus, Equations (9, 11) can be applied to estimate the crack initiation location, L_1. However, in practical application, after the crack is initialized and starts to propagate, the crack may propagate to random directions, and this assumption may not be true, and Equations (9, 11) may not be applicable to calculate the crack depth, a. To solve this challenge, based on measured strains from Sensors 1 and 2, Equations (9, 11) will be used to calculate the crack initialization location, L_1, and noted as $L_{1,\ t=0}$. For the next time interval, t=i, based on the measured strains and Sensor 1 and 2, the crack location, $L_{1,\ t=i}$ can be re-estimated. Thus, the angle of the crack away from the perpendicular direction ϕas shown in Fig. 2, can then be estimated as below:

$$\phi = \sin^{-1}(\Delta L/a) \tag{12}$$

where, ΔL is measured distance difference between $L_{1,\ t=0}$ and $L_{1,\ t=i}$ measurement. Therefore, based on Equations (9, 11, and 12), not only the crack location but also the crack propagation can be estimated based on the real-time measurements of the strains at the bottom of the pavement. Fig. 3 illustrates the flowchart of the developed crack detection algorithm.

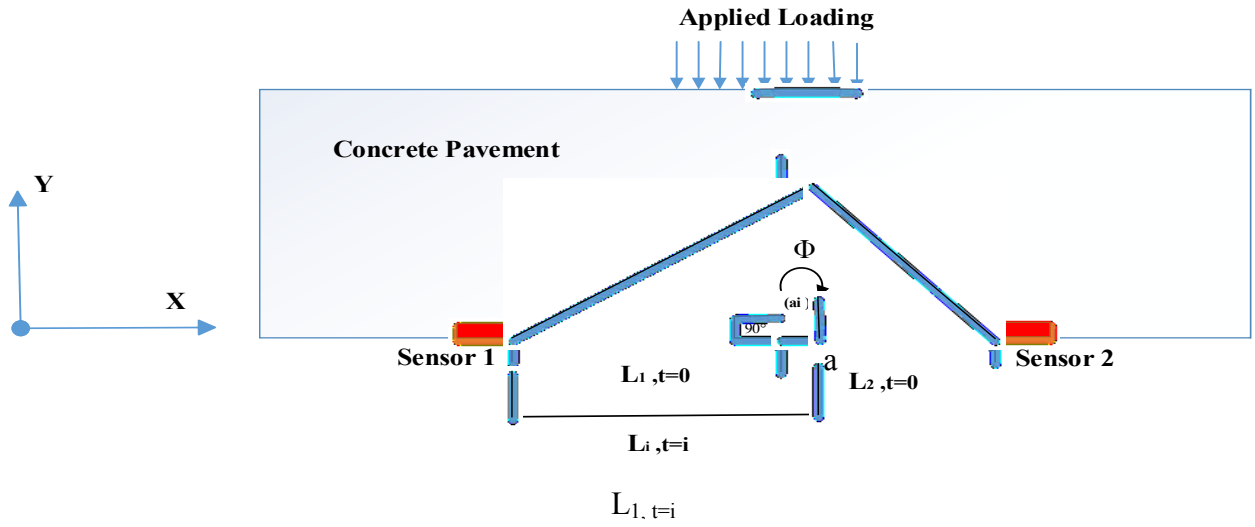

Fig. 2 Sensor locations vs. crack propagation in random directions after initiation

As shown in flowchart in Fig. 3., the applied stress on the structure and the detected strains from the in-pavement strain sensors will be used as input to this algorithm. These input will be feeded to equations (9,11) to calculate the real-time crack length and the crack locations. As long as the crack length becomes non-zero, the calculated crack location will be noted as the location when crack initiates, $L_{1,\ t=0}$. Equations (9, 11) will be used continuously to estimate the crack location at later time interval, i, which is noted as $L_{1,\ t=i}$ based on the measured strains. The difference between $L_{1,\ t=0}$ and $L_{1,\ t=i}$ will be calculated and input to Equation 12 together with the estimated crack length from Equations (10, 11) from time interval, i. Finally, Equation (12) will be used to estimate the crack directions at time interval, i, which will produce the crack progressing map along the bottom of the pavement.

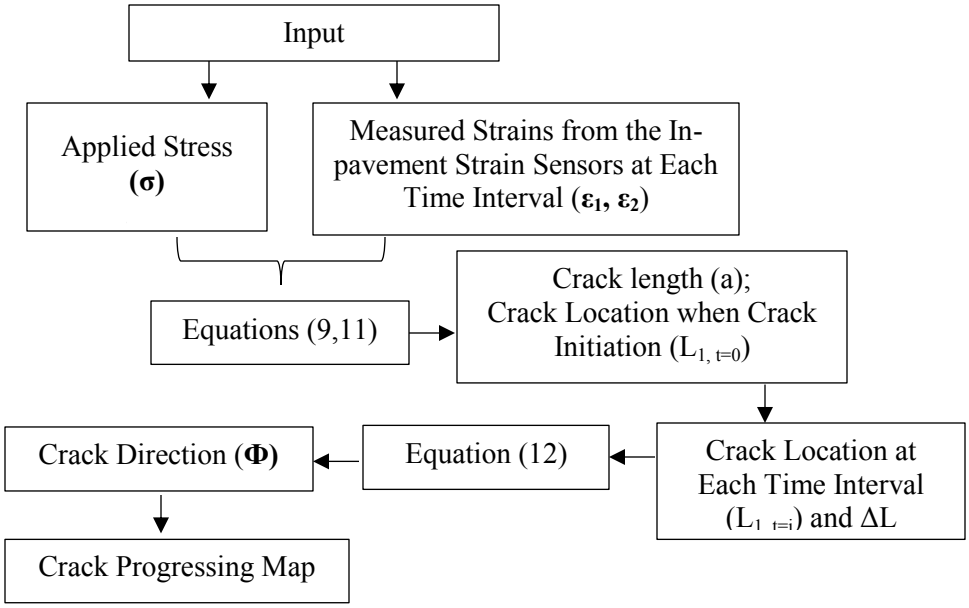

Fig. 3. flowchart for the developed crack detection algorithm

To demonstrate the feasibility of the developed approach above, the parametric study performed using MATLAB. Table 3 shows the mechanical properties of the material (concrete) simulated. The horizontal distance between the two sensors at the bottom of the pavement, L, was assumed to be 200 mm, and the crack was assumed to be perpendicular to the pavement surface in the analysis. Three cases were analyzed for the different crack distances away from Sensor 1, L_1, with 25mm, 50mm, and 100mm, as shown in Table 3 for crack locations analyzed for the three cases.

Table 2 Summary of mechanical characteristics of concrete

Parameter	**Value**
Elastic modulus, E	33.234 GPa
Compressive strength, σ_c	50 MPa
Tensile strength, σ_t	5 MPa

Table 3 Parametric study matrix

Case No.	**L_1 (mm)**	**L_2 (mm)**
1	25	175
2	50	150
3	100	100

Figures 4 (a~c) shows the simulated strain changes in the x-direction at Sensor 1 and Sensor 2 locations with different crack depth (a) for the three cases, respectively. When the crack is close to the sensor, for instance, 25mm and 50mm away from the Sensor 1, the strain increases as the crack propagating. On the other hand, when the crack is far away from the sensor, larger than 50mm, the strain decreases as the crack propagating. Thus, by tracking the pattern of strain changes measured on strain sensors, it is possible to quickly qualitatively locating the crack's location in respect of the sensor locations.

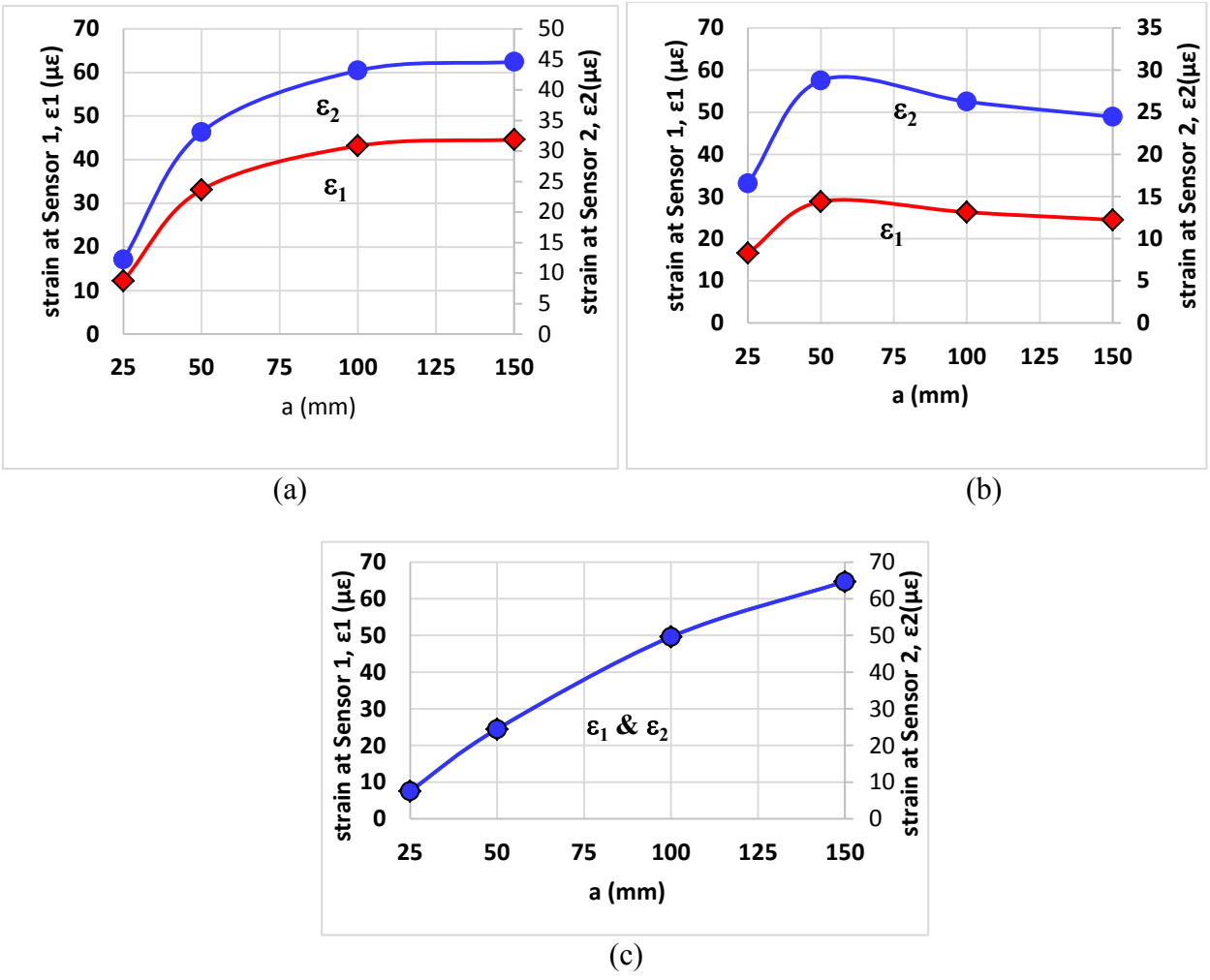

Fig. 4 Estimated strains at sensor locations for (a) Case 1, (b) Case 2, and (c) Case 3

3 Experimental Study and Discussions

To validate the developed crack detection, an algorithm using embedded sensors for pavements, experiments were performed in the laboratory. Table 4 shows the detail concrete mix design with w/c of (0.35) used in this study.

Table 4 Concrete composition

Materials	**Amount (kg/m^3)**
Cement (Kg)	25
Coarse Aggregate –Gravel pass sieve opening 19 mm (Kg)	10
Coarse Aggregate –Gravel pass sieve opening 16 mm (Kg)	10
Coarse Aggregate –Gravel pass sieve opening 12.5 mm (Kg)	12
Coarse Aggregate –Gravel pass sieve opening 9.5mm (Kg)	16.5
Fine Aggregate-Sand pass sieve opening 4.75 mm (Kg)	12
Fine Aggregate-Sand pass sieve opening 0.075 mm (Kg)	17.5
Water (Kg)	8.7

3.1 Mechanical Property of Tested Concrete

Before the crack detection on lab specimens, material characterization tests were conducted. These included compression, tensile, and flexural strength tests. Three samples tested for each strength test. Figure 5 (a) shows the test setup for the compression strength test. The cylindrical specimens had nominal dimensions of 152.4 mm × 304.8 mm, which tested at the age of 28 days. Loading was applied continuously until specimen rupture following ASTM C39. Figure 5 (b) shows the test setup for the tensile strength. For the tensile strength by diametric compression test, the prismatic specimens had nominal dimensions of 50.5 mm × 50.8 mm ×304.8 mm specimens, which were also tested at the ages of 28 days, fractured in a universal press. The cracking strength is lower than the tensile strength of concrete. Crack propagation governed by the cracking strength [28].

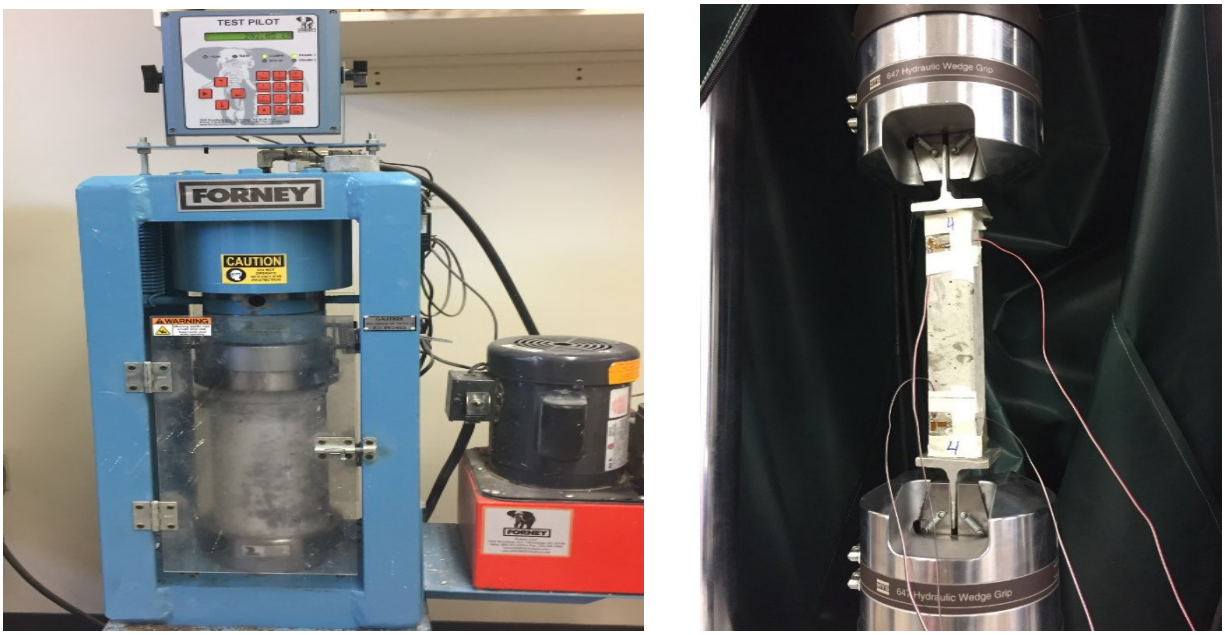

(a) (b)

Fig.5 Compression Strength Test (a) and Tensile Strength Test (b)

Also, flexural strength tests were performed on the tested concrete, as shown in Figure 6. The tested prismatic specimens had nominal dimensions of 152.4 mm × 152.4 mm × 508 mm, which subjected to rupture at the ages of 28 days following ASTM C78. Based on the applied loads and the dimension of the tested specimen, the flexural strength calculated as [29]:

$$R = \frac{\mathrm{P}l}{\mathrm{bd}^2} \tag{13}$$

where R is the modulus of rupture (MPa), P is the applied load (N), l is the distance between the support (mm), b is the average specimen width at the rupture section (mm), and d is average specimen height at the rupture section (mm).

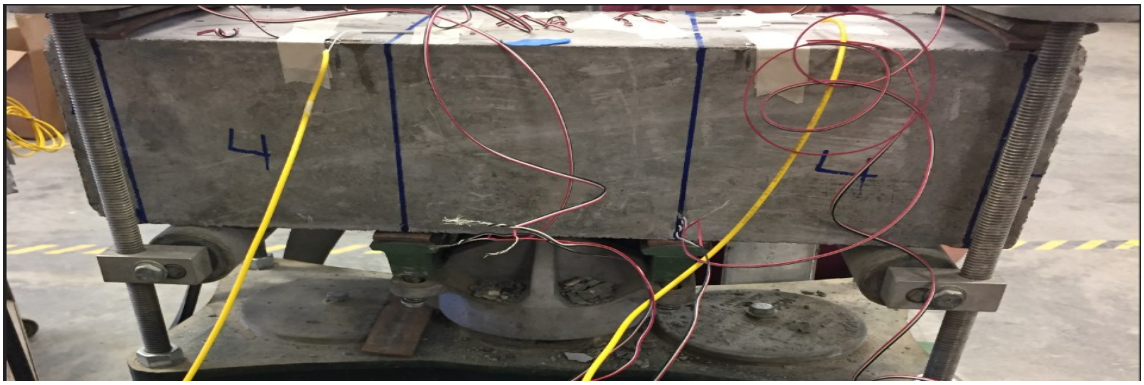

Figure 6 Flexural Strength Test

Table 5 presents the results obtained from the mechanical property tests of the used concrete. The average mechanical properties will be used in Equations (9~12) to estimate the strains for crack detection using discrete strain sensors.

Table 5 Mechanical Property of the Tested Concrete

Sample No.	Compression strength (MPa)	Tensile strength (MPa)	Flexural Strength (MPa)
1	45	2.5	5.3
2	44	1.8	5.8
3	46	2.0	6.0
Average	45	2.1	5.7

3.2 Crack Detection and Discussions

To test the developed crack detection system in this paper, three concrete beam specimens with nominal dimensions of 152.4 mm × 152.4 mm × 508 mm, were made in the laboratory, and three-point loading tests were performed on each beam to create cracks. On the bottom surface of each specimen, four strain gauges were attached. Figure 7(a) shows the schematic of the sensor layout at the bottom surface of the beam, and Figure 7(b) illustrates one specimen with sensors installed at the desired locations. All the detected strains were collected using data acquisition and recorded using a personal computer for post-experiment analysis.

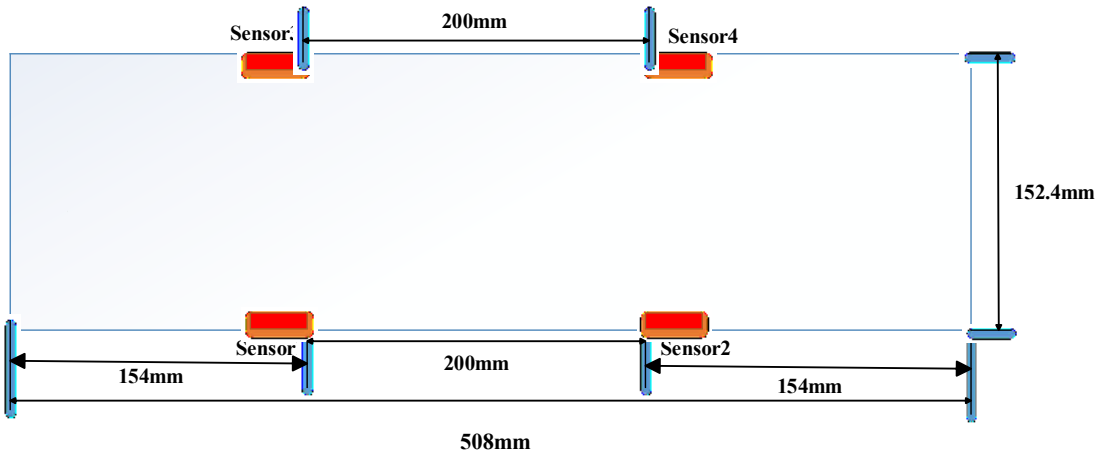

(a)

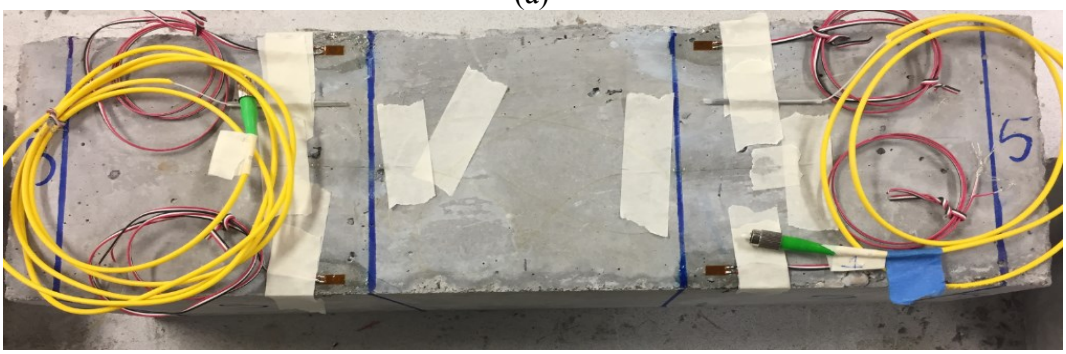

(b)

Fig.7 Schematic (a) and photo of the sensor layout (b)

Figures 8 (a, b) illustrate the measured strains from the strain gauges of Sample 1 during the three-point loading tests. Based on Equations (9, 11, and 12) and with the measured strains from Sensor 1 and 2, the crack location and crack propagation (crack depth) on the front surface of the specimen were calculated as shown in Fig. 8 (a). In Figure 8 (a), X-axis is the distance between the identified crack to Sensor 1 and Y-axis if the crack depth pattern changes in the vertical direction. The actual cracks were also measured from Fig. 9 (a) to compare with the estimation of crack patterns based on the sensor readings. Fig. 9 (b) also shows the photo of the crack pattern after cracking for Sample 1. For Sample 1, the maximum variance between the crack patterns detected from the sensors is within 8 mm, which is 5 % of crack estimation error.

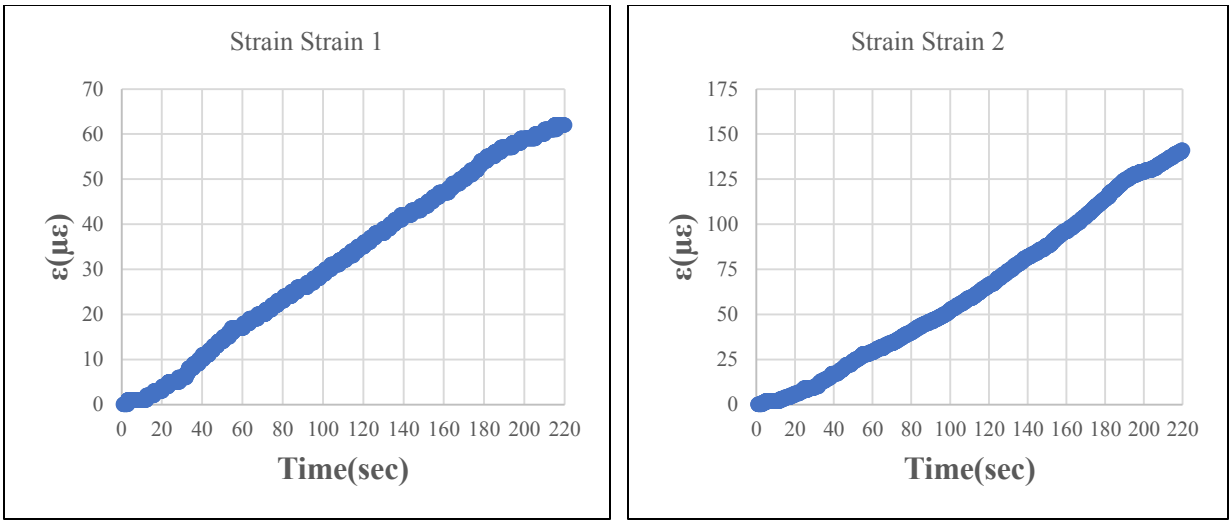

(a) (b)

Fig. 8 Measured strains from the Sensor 1 (a) and Sensor 2 (b) of Sample 1

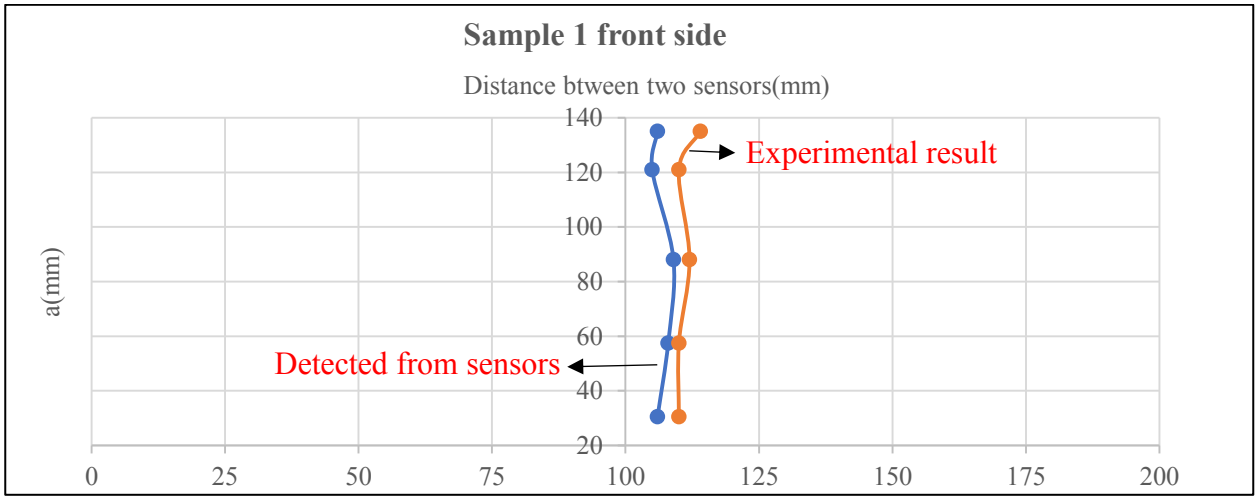

(a)

(b)

Fig. 9 Comparison of detected crack compared with reference crack (a) and photo of after cracking (b) for Sample 1

Fig.10 (a, b) illustrates the measured strains from the strain gauges of Sample 2 during the flexural strength tests and Figure 11 (a) is the comparison between crack location and crack propagation (crack depth) in the front surface estimated using sensors and the actual cracks as shown in Fig. 11 (b). For Sample 2, the maximum variance between the crack patterns detected from the sensors is 46 mm, which is 30.1 % of crack estimation error.

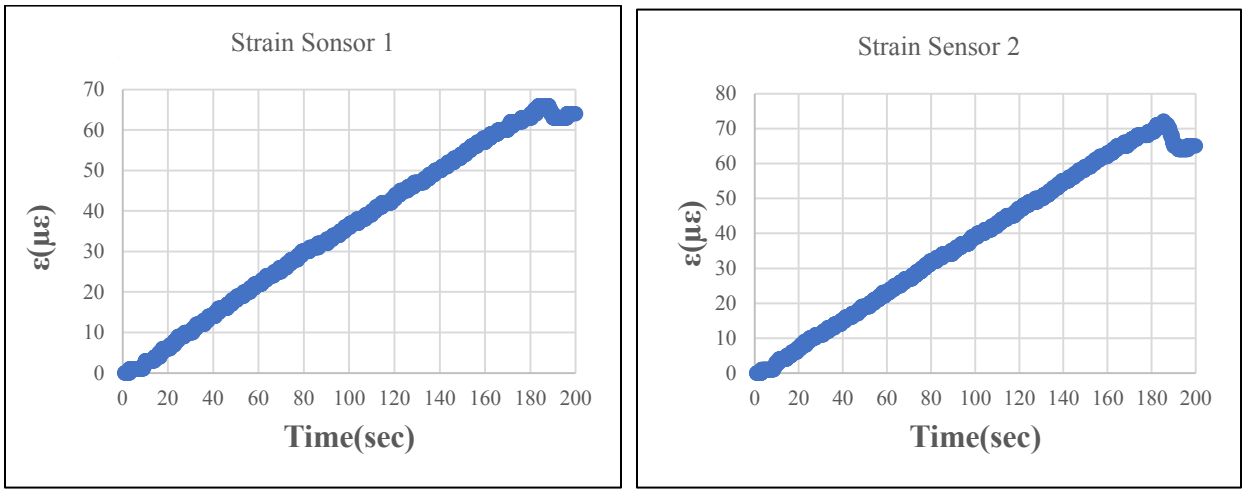

(a) (b)

Fig. 10 Measured strains from the Sensor 1 (a) and Sensor 2 (b) of Sample 2

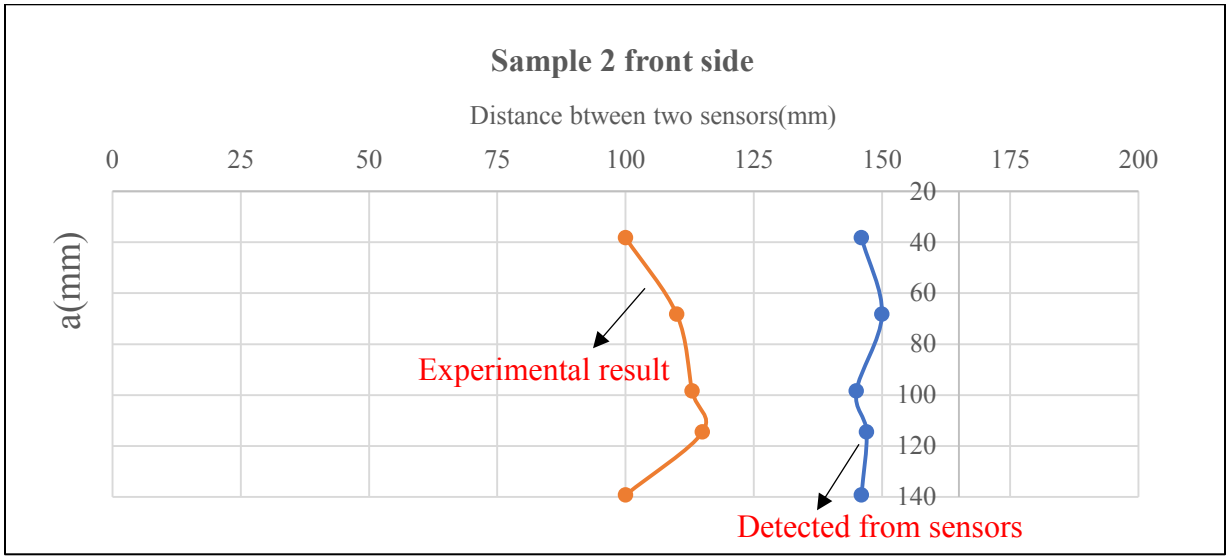

(a)

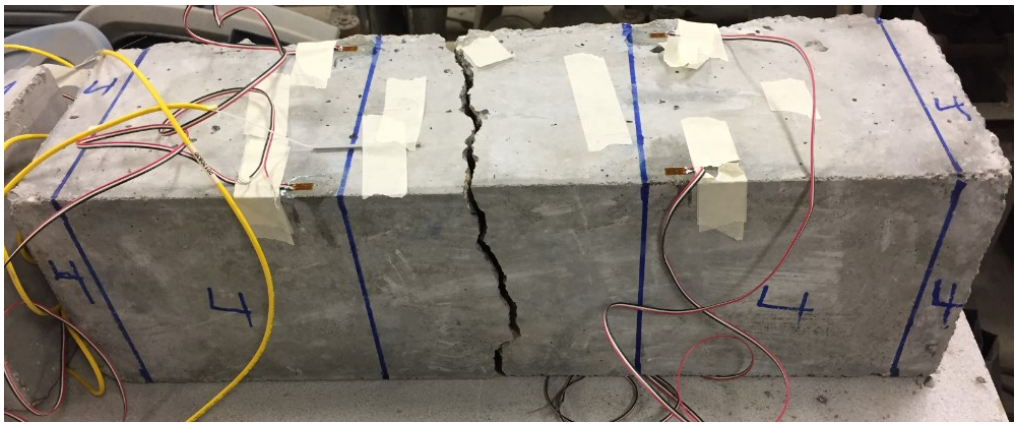

(b)

Fig. 11 Comparison of detected crack compared with reference crack (a) and photo of after cracking (b) for Sample 2

Fig. 12 (a, b) illustrates the measured strains from the strain gauges of Sample 3 during the flexural strength tests and Fig. 13 (a) represents the comparison between crack location and crack propagation (crack depth) in the front surface estimated using sensors and the actual cracks, as shown in Fig. 13 (b). For Sample 3, the maximum variance between the crack patterns detected from the sensors is within 27 mm, which is 17.71% of crack estimation error.

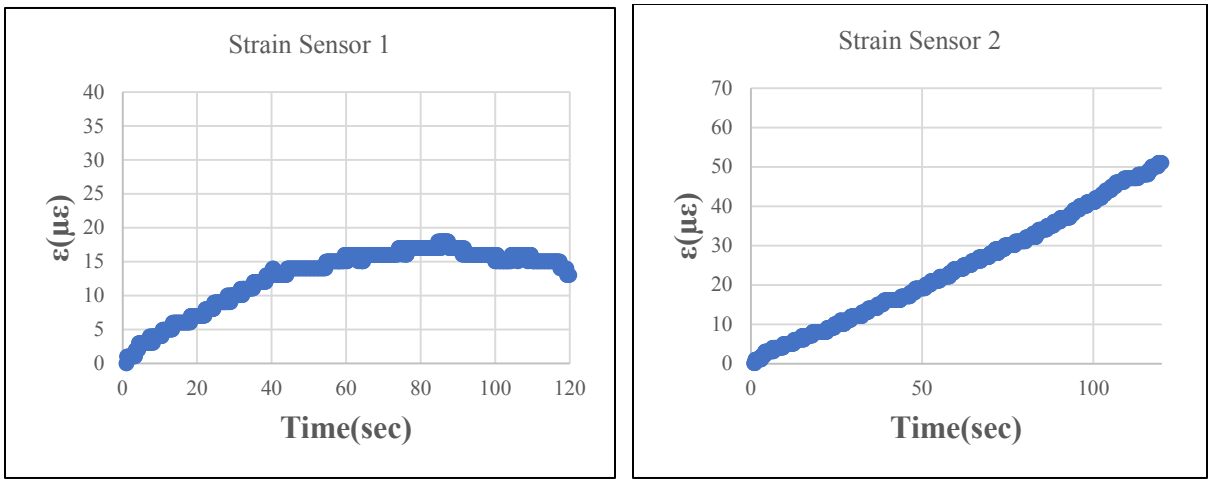

(a) (b)

Fig.12 Measured strains from the Sensor 1 (a) and Sensor 2 (b) of Sample 2.

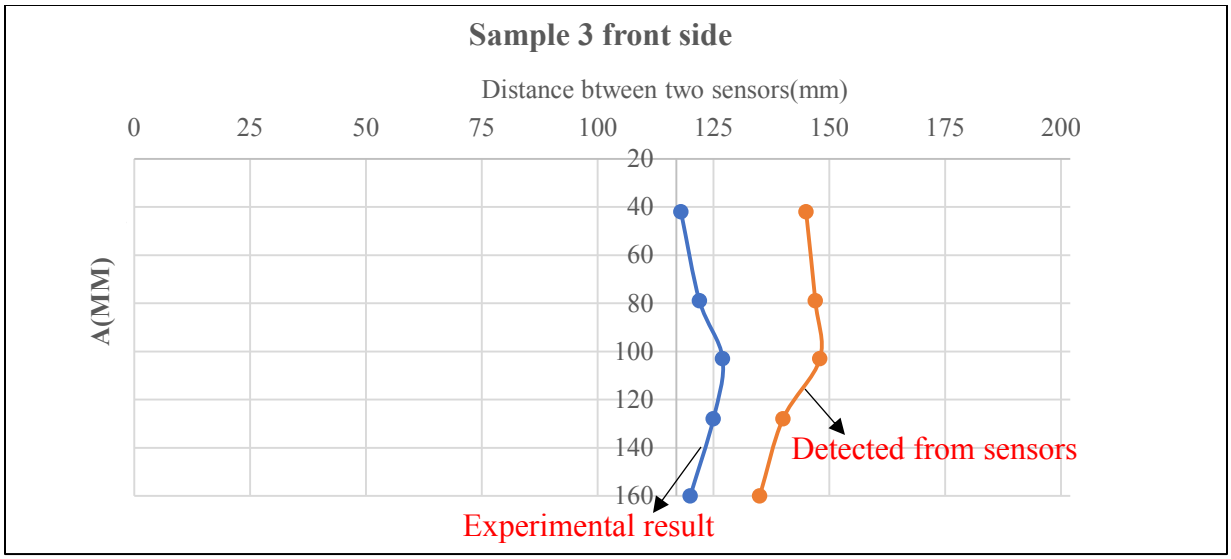

(a)

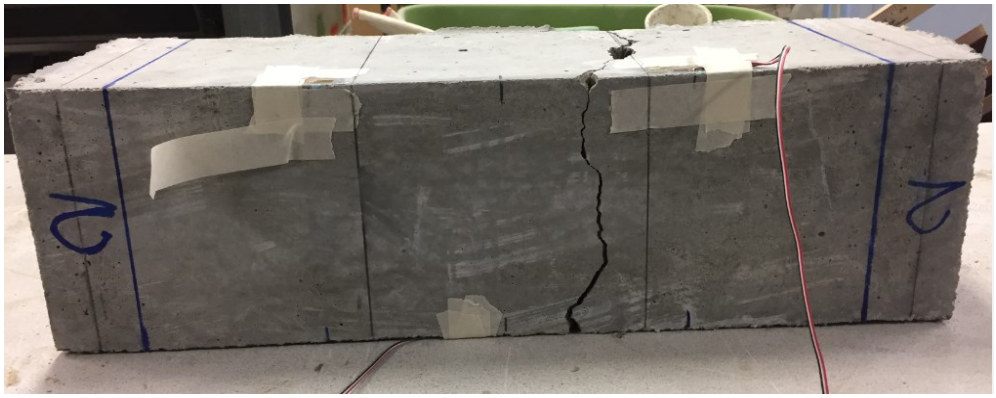

(b)

Fig. 13 Comparison of detected crack compared with reference crack (a) and photo of after cracking (b) for Sample 3

Table 6 summarized the comparison of maximum variance of crack location from Sensor $_1$, L_1, calculated from developed analytic analysis and measured from experimental results from all three samples. From Table 6, Fig. 9 (a), 11 (a), and 13 (a), it can be seen that the average variance between the crack pattern detected using the discrete sensors on the bottom of the concrete beam and the actual crack pattern for all three samples is 17.6 %, indicating a very promising crack detection approach for field internal crack detection.

Table 6 Comparison of maximum variance of crack location from Sensor $_1$, L_1, calculated from developed analytic analysis and measured from experimental results

Sample Number	**Analytical solution calculated from developed sensing plan** (mm)	**Experimental result measured from the experiments** (mm)	**Maximum error (%)**
Sample 1	106	114	5
Sample 2	146	100	30.1
Sample 3	120	135	17.7
Average			17.6

4 Conclusions and Future Work

In this study, an innvative approach is introduced to use minimum numbers of discrete strain sensors installed at the bottom of the pavement to detect bottom-up cracks. The developed algorithm with the sensor network can be used to locate crack and detect the crack depth and propagating pattern based on linear elastic fracture mechanics. Experimental and analytical investigation results showed that the comparison between crack pattern detected using the discrete sensors on the bottom of the concrete beam and the actual crack pattern had an average measurement accuracy of 82.4%. The consequences of this study can not only be used to verify, control, assess, and understand the actual behavior of hidden cracks of the concrete pavements, but also other concrete structures with limited accessbility. The detected crack progressing patterns and trends in concrete pavement can assist to improve the concrete pavement design process for a more accurate estimation of material properties such as such modulus of elasticity (E) and poisons ratio (υ), followed by reduced strength and stiffness of concrete. Future efforts will be directed to perform field testing inside the pavement to validate the field-testing challenges and also further quantitatively locate multiple cracks using discrete sensor networks.

Acknowledgments: The U.S. Department of Transportation partially supported this study under the agreement No.69A35517477108 through Mountain-Plains Consortium Project No. MPC-547 and NSF Award No. 1750316.

REFERENCES

[1] Broomfield, J. P. Corrosion of steel in concrete: understanding, investigation and repair. CRC Press, 2003.
[2] Merritt, D. K., McCullough, B. F., and Burns, N. H. Construction and preliminary monitoring of the Georgetown, Texas precast prestressed concrete pavement. Center for Transportation Research, the University of Texas at Austin, 2001.
[3] Taheri, S. "A review on five key sensors for monitoring of concrete structures." Construction and Building Materials 204 (2019): 492-509.
[4] Benedetto, A. "A three dimensional approach for tracking cracks in bridges using GPR." Journal of Applied Geophysics 97 (2013): 37-44. DOI10.1016/j.jappgeo.2012.12.010
[5] Luburić, I., Perić, Z., and Šesnić, S. "Electromagnetic modeling of the GPR response to the pipe system set in the concrete slab." In 2017 25th International Conference on Software, Telecommunications and Computer Networks (SoftCOM), pp. 1-5. IEEE, 2017. DOI: 10.23919/SOFTCOM.2017.8115531 .
[6] Scullion, T. and Saarenketo, T. "Applications of Ground Penetrating Radar technology for network and project level pavement management systems." In Fourth International Conference on Managing Pavements, vol. 1. 1998.
[7] Fernandes, F. M., and Pais, J. C. "Laboratory observation of cracks in road pavements with GPR." *Construction and Building Materials* 154 (2017): 1130-1138.
[8] Birtwisle, A., and Utsi, E. "The use of ground penetrating radar to detect vertical subsurface cracking in airport runways." In Proceedings of the 12th International Conference on Ground Penetrating Radar (GPR2008), Birmingham, UK. 2008.
[9] Tong, Z., Yuan, D., Gao, J., Wei, Y., and Dou, H. "Pavement-distress detection using ground-penetrating radar and network in networks." *Construction and Building Materials* 233 (2020): 117352.
[10] Choi, P., Kim, D. H., Lee, B. H., and Won, M. C. "Application of ultrasonic shear-wave tomography to identify horizontal crack or delamination in concrete pavement and bridge." Construction and Building Materials 121 (2016): 81-91
[11] Khazanovich, L., Velasquez, R., and Nesvijski, E. G. "Evaluation of top-down cracks in asphalt pavements by using a self-calibrating ultrasonic technique." Transportation research record 1940, no. 1 (2005): 63-68.
[12] Tigdemir, M., Kalyoncuoglu, S. K. and Kalyoncuoglu, U. Y. "Application of ultrasonic method in asphalt concrete testing for fatigue life estimation." NDT & E International 37, no. 8 (2004): 597-602.
[13] Khazanovich, L., Velasquez, R., and Nesvijski, E. G. "Evaluation of top-down cracks in asphalt pavements by using a self-calibrating ultrasonic technique." Transportation research record 1940, no. 1 (2005): 63-68.
[14] Cook, K., Garg, N., Singh, A., and Flynn, M. "Detection of Delamination in the HMA Layer of Runway Pavement Structure Using Asphalt Strain Gauges." Journal of Transportation Engineering 142, no. 11 (2016): 04016047.
[15] Zhang, Z., Huang, Y., Palek, L., Strommen, R., and Worel, B., “Glass fiber reinforced polymer packaged fiber

Bragg grating sensors for ultra-thin unbonded concrete overlay monitoring," Structural Health Monitoring, October 13, 2014, 1475921714554143.

[16] Bao, Y., Tang, F., Chen, Y., Meng, W., Huang, Y., and Chen, G. "Concrete pavement monitoring with PPP-BOTDA distributed strain and crack sensors." Smart Structures and Systems 18, no. 3 (2016): 405-423. DOI: http://dx.doi.org/10.12989/sss.2016.18.3.405.
Monitoring." Structural Health Monitoring 14, no. 1 (2015): 110-123.

[17] Wu, Z. S., Xu, B., Takahashi, T., and Harada, T. "Performance of a BOTDR optical fibre sensing technique for crack detection in concrete structures." Structures and Infrastructure Engineering 4, no. 4 (2008): 311-323.

[18] Chapeleau, X., Blanc, J., Hornych, P., Gautier, J. L., and Carroget, J. "Assessment of cracks detection in pavement by a distributed fiber optic sensing technology." Journal of Civil Structural Health Monitoring 7, no. 4 (2017): 459-470. DOI.https://link.springer.com/article/10.1007/s13349-017-0236-5#citeas

[19] Patil, P. K. and Patil, S. R. "Structural health monitoring system using WSN for bridges." In *2017 International Conference on Intelligent Computing and Control Systems (ICICCS)*, pp. 371-375. IEEE, 2017.

[20] Maeijer, K. D., Patricia, G. L., Vuye, C., Voet, E., Vanlanduit, S., Braspenninckx, J., Stevens, N. and Wolf, J. D., "Fiber Optics Sensors in Asphalt Pavement: State-of-the-Art Review." *Infrastructures* 4, no. 2 (2019): 36.

[21] Srinivasan, A. V., and McFarland, D. M. "Smart structures, analysis and design." (2001): 1212-1212.

[22] Alshandah, M., Huang, Y., Lu, P., and Tolliver, D. "Bottom-up crack detection in concrete pavements using in-pavement strain sensors." In Sensors and Smart Structures Technologies for Civil, Mechanical, and Aerospace Systems 2018, vol. 10598, p. 105982I. International Society for Optics and Photonics, 2018.

[23] Sahoo, A. K., Dubey, R. N., and Pandey, M. D. "Crack Induced Stress and Deformation Field." Transaction, SMiRT 19 (2007).

[24] Rice, J. "Elastic fracture mechanics concepts for interfacial cracks." J. Appl. Mech.(Trans. ASME) 55, no. 1 (1988): 98-103.

[25] Rooke, D. P., and Cartwright, D. J. "Compendium of stress intensity factors." Procurement Executive, Ministry of Defence. H. M. S. O. 1976, 330 p(Book). (1976).

[26] Tada, H., Paris, P. C., and Irwin, G. R. "The stress analysis of cracks." Handbook, Del Research Corporation (1973).

[27] Anderson, T. L. Fracture mechanics: fundamentals and applications. CRC press, 2017.

[28] Zhang, J., and Liu, Q. "Determination of concrete fracture parameters from a three- point bending test." Tsinghua Science and Technology 8, no. 6 (2003): 726-733.

[29] ASTM, C78. "Standard test method for flexural strength of concrete (using simple beam with third-point loading)." In American Society for Testing Materials. 2010.